ChemComm

COMMUNICATION

View Article Online
View Journal | View Issue

Cite this: *Chem. Commun.*, 2020, **56**, 2865

Received 8th October 2019,
Accepted 31st January 2020

DOI: 10.1039/c9cc07722g

rsc.li/chemcomm

Low temperature dissociation of CO on manganese promoted cobalt(poly)†

Ryan A. Ciufo,[ab] Sungmin Han,[a] Michael E. Floto,[a] Graeme Henkelman[ab] and C. Buddie Mullins*[ac]

We observe that metallic manganese alloyed with polycrystalline cobalt promotes the dissociation of CO. Increasing coverages of Mn on Co facillitate stronger molecular CO binding energies and stronger C(ad) + O(ad) binding energies. These findings show the role of metallic manganese in promoting model Co Fischer–Tropsch catalysis.

The Fischer–Tropsch (FT) process has been extensively studied for its use in producing hydrocarbons of various lengths from carbon monoxide and hydrogen gas.[1–3] Due to its tailorability, the FT process has shown promise and continues to compete with the energy and petrochemical industries.[1,2,4] One area where FT shows much promise for growth is for the production of lower olefins. The production of lower olefins is one of the most important chemical processes in the world today for their use as chemical feedstocks for a number of industries. Most lower olefins are produced through cracking of a range of hydrocarbon feedstocks such as naphtha, gas oil or light alkanes. Due to the energy cost of the cracking process and the limited petroleum reserves, there has been a push to develop alternative methods of deriving lower olefins. The FT to olefins process has shown the ability to break the traditional Anderson–Schultz–Flory (ASF) product distribution expected with Fischer Tropsch synthesis to produce lower olefins from syngas while limiting methane production.[5,6]

Among the few catalysts shown to break the ASF distribution are manganese promoted cobalt catalysts. Mn/Co systems have been shown to promote low chain olefin selectivity, C_{5+} selectivity, affinity for long chain alcohol synthesis, and increase overall intrinsic activity.[7–11] In addition to promoting FT activity, $Co_xMn_{1-x}O$ mixtures were shown by Zhong *et al.* to form Co_2C nanoprisms under reaction conditions, which promoted the synthesis of lower olefins while limiting methane production to approximately 5%.[12] Additional works by Morales *et al.* used a number of characterization techniques (EXAFS, XANES, STEM-EELS, XAS) to study the nature of Co, Mn and Ti in $Mn/Co/TiO_2$ catalysts.[13–15] Their studies showed the very diverse and complex states of Mn present in Mn/Co alloys (including Mn, Mn(II), Mn(III) and Mn(IV)) and the influence of synthesis and pre-treatment on the state of Mn and Co. Recently, theoretical work by Pederson, *et al.*, showed that metallic Mn with Co(111) produced similar selectivity as compared to their experimental work with MnO promoted Fischer Tropsch catalysts.[7] This work suggested that metallic alloyed Mn may produce similar results as Mn_xO_y for promoting Co FT catalysts. In this paper, we report our investigation of the interaction of CO with metallic Mn promoted cobalt polycrystalline surfaces by employing molecular beam techniques in ultra-high vacuum (UHV). We show, using surface science techniques and density functional theory (DFT), that the addition of metallic Mn as a promoter to Co facilitates dissociative adsorption of CO by stabilizing $C_{(ad)} + O_{(ad)}$ intermediates. These findings show the role of Mn in a model FT system, and provide insight into the unique activity and selectivity of Mn/Co Fischer–Tropsch catalysts.

To study the uptake of CO on our surfaces, we performed King and Wells (K + W) experiments by impinging a molecule beam of CO on each of our Mn/Co samples at 100 K.[16,17] All K + W experiments were performed until the surface was fully saturated with CO (Fig. S1, ESI†). Following uptake experiments, CO temperature programmed desorption (TPD) spectra were obtained (Fig. 1a). As seen in Fig. 1a, CO yields two major desorption features on the 0.0 monolayer (ML) Mn/Co surface (*i.e.*, pure cobalt surface – green line) at ~400 K and ~640 K. The feature near 400 K is the result of molecular CO desorption, while the feature near 640 K is the result of $C_{(ad)} + O_{(ad)}$ recombinatively desorbing as CO.[17,18] The feature seen between 100 K and 150 K is the result of desorption from other parts of our probe. It is seen that as the coverage of Mn is increased, there is an increase in intensity of the recombinative desorption feature and corresponding decrease in

[a] *Department of Chemistry, University of Texas at Austin, Austin, Texas 78712, USA. E-mail: mullins@che.utexas.edu*
[b] *The Oden Institute for Computational Engineering and Science, University of Texas at Austin, Austin, Texas 78712, USA*
[c] *The McKetta Department of Chemical Engineering, Texas Materials Institute, Center for Electrochemistry, University of Texas at Austin, Austin, Texas 78712, USA*

† Electronic supplementary information (ESI) available. See DOI: 10.1039/c9cc07722g

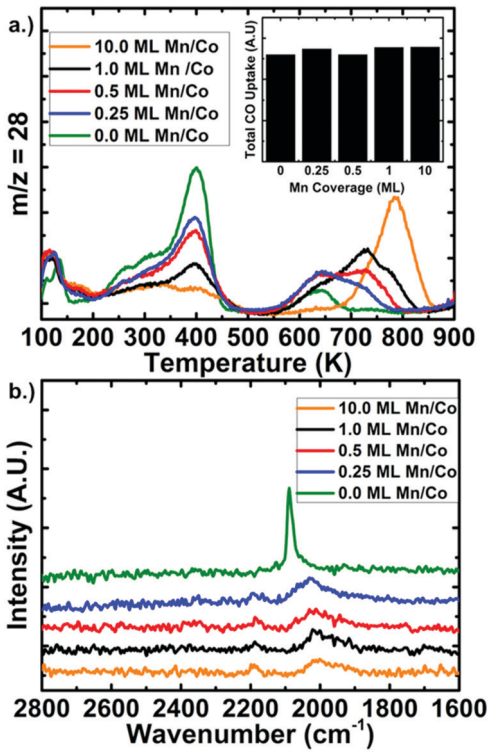

Fig. 1 (a) CO TPD for various coverages of Mn on Co(poly) after CO K + W at 100 K. (a, inset) total uptake of CO from King and Wells experiments (b) RAIRS performed at 100 K after CO impingement at 100 K for various coverages of Mn on Co(poly).

the molecular desorption feature. The recombinative desorption peak shifts to higher temperatures with increased Mn coverage (~775 K for 10 ML Mn/Co). These changes denote an increased affinity for Mn covered surfaces to dissociate CO and suggest that intermediate $C_{(ad)}$ and $O_{(ad)}$ are stabilized on the Mn promoted surfaces. As the coverage of Mn on Co increases, new recombinative features appear at higher temperatures. For example, the 1.0 ML Mn/Co surface (Fig. 1, black line) shows three distinct recombinative features at ~640 K, ~725 K, and ~775 K. We attribute these three desorption features to the alloyed nature of our Mn/Co surfaces. The peak at ~640 K is characteristic of recombinative desorption from cobalt rich regions.[17,18] For high coverages of Mn (~10 ML), a distinct feature is seen at ~775 K. We attribute this feature to recombinative desorption from regions rich in metallic Mn. Lastly, we attribute the feature seen at 725 K to desorption from mixed cobalt–manganese regions.

To probe the nature of the interaction of adsorbed CO on our Mn/Co surfaces, reflection absorption infrared spectroscopy (RAIRS) was performed at 100 K after CO was impinged at 100 K (Fig. 1b). For a 0.0 ML Mn/Co surface, a sharp feature is seen at 2089 cm^{-1} corresponding to saturated linearly adsorbed molecular CO (Fig. 1b, green curve).[10,19] As Mn coverage is increased, it is seen that the molecular CO vibration decreases in intensity, broadens, and shifts to lower wavenumbers. The decrease in intensity suggests a decrease in the coverage of molecular CO on our surfaces. The shift and broadening of the CO vibrational feature with increased Mn aligns with past studies that show decreased coverages of molecular CO are more strongly bound to the surface.[20,21] Since the total uptake of CO on all Mn/Co surfaces was seen to be nearly identical (Fig. 1a, inset), these findings suggests that on Mn promoted surfaces, CO exists in both a molecular and dissociated state (as $C_{(ad)}$ + $O_{(ad)}$) at 100 K. As Mn coverage is increased, the fraction of molecular CO decreases, while the fraction of dissociated CO increases. This trend also corresponds to the data in Fig. 1a, where increased Mn coverages show decreased molecular CO desorption and increased recombinative desorption. It is important to note that no feature is seen for CO interactions with MnO (between 1700–1600 cm^{-1}),[10,22] suggesting that Mn exists as metallic Mn in our system.

To gain a deeper understanding of the nature of the CO dissociation on our surfaces, we performed uptake experiments with our sample at elevated temperatures. First, we impinged a molecular beam of CO while holding the sample at various temperatures and allowed the sample to cool to 100 K. RAIRS and TPD experiments were then performed (Fig. 2). In Fig. 2a, TPD after impinging CO at 500 K (above the molecular desorption temperature but below the recombinative desorption temperature) shows a similar recombinative desorption feature compared to the same experiment performed with the sample at 100 K (Fig. 2a, black curve). Following impinging at 500 K, the sample was cooled to 100 K and RAIRS was performed (Fig. 2b, red curve). No molecular CO RAIRS feature is seen for the experiments performed above 500 K. The lack of molecular

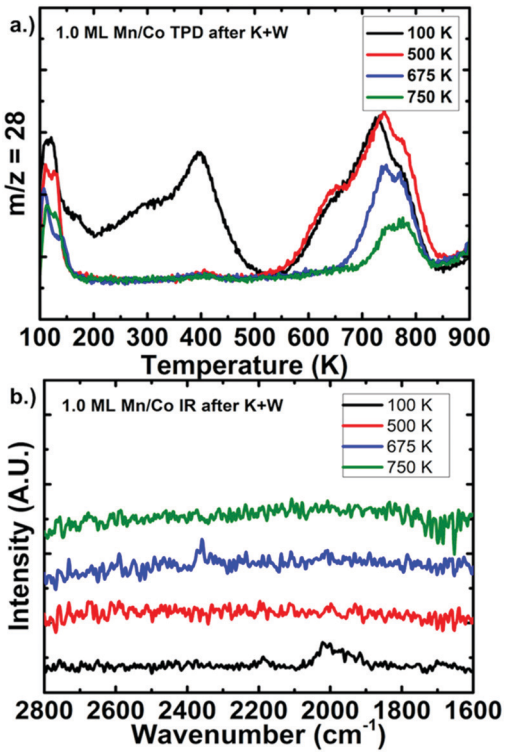

Fig. 2 (a) CO TPD from 1.0 ML Mn/Co after CO K + W at various temperatures. (b) RAIRS at 100 K after CO K + W at various temperatures on 1.0 ML Mn/Co.

CO vibrations after exposure at 500 K and the similarity between the recombinative desorption features from the exposures at 100 K and 500 K further suggests that the desorption features seen above 650 K are from recombinative desorption rather than a strongly bound molecularly adsorbed CO entity. When the sample was held at 675 K and 750 K (Fig. 2a blue and green curves, respectively), a decrease in the recombinative feature is observed due to the sample being held above the recombinative desorption temperature. At 675 K and 750 K, the recombinative desorption features at 640 K and 725 K decrease. As with the experiments described above at 500 K, after impinging CO onto the sample at 675 and 750 K, no molecular CO was observed with RAIRS (Fig. 2b).

Auger electron spectroscopy was also employed to characterize our surface. As seen in Fig. 3a, the AES spectra after evaporating Mn and annealing to 900 K at 5 K s^{-1} show Mn LMM features (540 eV, 594 eV, and 640 eV). The Mn features increase in intensity with increasing Mn coverages. Inversely, the Co LMM features (660 eV, 717 eV, and 783 eV) decrease with increasing Mn coverages. Fig. 3b shows Auger spectra for a typical 10 ML Mn/Co surface annealed to 900 K (orange curve), for an unannealed 10 ML Mn/Co sample (magenta curve), and a 10 ML Mn/Co annealed sample following CO K + W at 100 K and TPD to 900 K (black curve). It is seen that the freshly prepared, unannealed sample displays large Mn features and minute Co LMM features. Upon annealing, the Co features reappear, and the Mn features decrease in intensity. The change in the Mn:Co Auger intensity shows that the Mn is migrating into the Co surface and alloying with the Co(poly). This aligns with previous work by Iijima, *et al.*, which showed a high diffusivity for Mn in Co.[23,24] An annealed 10 ML Mn/Co surface was impinged with CO at 100 K and a TPD was performed to 900 K. An Auger spectrum was taken of this "used" 10 ML Mn/Co sample (Fig. 3b, black line). The difference between the Auger before (Fig. 3b, orange curve) and after experiment (Fig. 3b, black curve) is negligible, indicating that the surface composition has not changed over the course of the experiment. Lastly, Auger was performed on two Mn/Co surfaces (10 ML and 0.5 ML) which were intentionally oxidized using different methods. In these curves, a clear oxygen feature is seen, which corresponds to Mn_xO_y formation (Fig. S3, ESI†). Importantly, since no oxygen features appear in any of the annealed Co/Mn spectra (nor in the "used" spectra), we are confident that Mn is predominantly in the metallic state before and after exposure to CO. Lastly, upon heating the oxidized Mn_xO_y/Co surface, trace desorption of $m/z^+ = 55$ is detected above 500 K, indicating the desorption of Mn_xO_y (most likely from MnO_2). This is not detected in any of the metallic Mn/Co samples, further indicating the metallic nature of Mn on our surfaces.

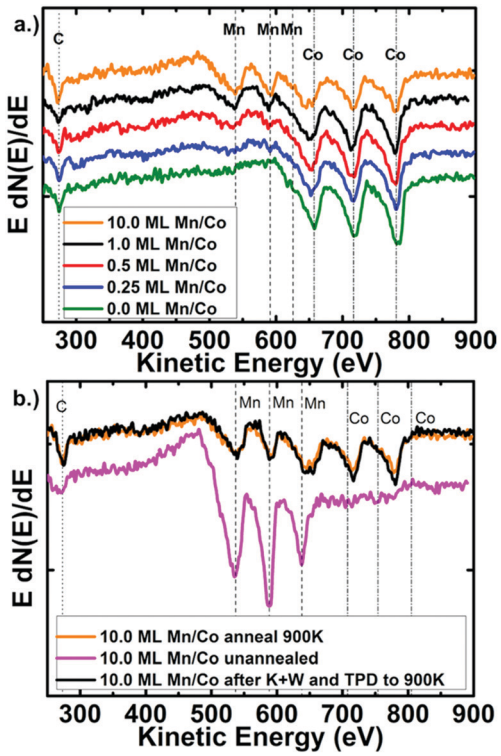

Fig. 3 (a) AES spectra for various coverages of Mn on Co(poly). (b) Auger spectra before annealing, after annealing and after experiment for 10 ML Mn/Co.

To better understand the nature of the interaction between our surfaces and CO, we conducted DFT calculations. In contrast to earlier work by Pederson *et al.*,[7] we chose to study the HCP(0001) facet of Cobalt instead of the FCC(111) facet. HCP cobalt is the dominant phase present at low temperatures and the (0001) facet has the lowest surface energy.[25,26] Therefore, we expect HCP(0001) to be a predominant facet in our low temperature studies of Co(poly). Mn is found naturally in the $I\bar{4}3m$ space group, but for the purpose of this study was considered as a surface alloy with HCP Co.[27] It should be noted that Mn readily alloys with both HCP and FCC cobalt, and that Mn does not appear to influence the phase stability of the cobalt.[23,28] The systems were modelled as a 4-layer slab and (2 × 2) surface unit cell. The binding energies of molecular CO and dissociated $C_{(ad)}$ + $O_{(ad)}$ were calculated for all surfaces relative to gas phase CO and the respective clean surface. For 0.25 ML Mn/Co and 0.5 ML Mn/Co, there were 4 and 6 surface configurations possible, respectively (Fig. S2, ESI†). For the 0.25 and 0.5 ML systems, the mean binding energies were reported along with the standard deviation (Fig. 4 blue and red curves).

As seen in Fig. 4, an increase in molecular CO binding energy of ~0.2 eV was seen for all Mn/Co models compared to 0.0 ML Mn/Co with the exception of the 0.5 ML Mn/Co surface, which had a larger increase of ~0.35 eV. For the adsorption of dissociated $C_{(ad)}$ + $O_{(ad)}$, clean Co(0001) shows the weakest binding. As Mn coverage increases, the binding energy of $C_{(ad)}$ + $O_{(ad)}$ increases, with 1.0 ML Mn/Co having the strongest $C_{(ad)}$ + $O_{(ad)}$ binding energy of −2.59 eV. For 2.0 ML Mn/Co, the dissociated binding energy is ~0.35 eV weaker than on 1.0 ML Mn/Co. We believe that this decrease in $C_{(ad)}$ + $O_{(ad)}$ binding energy for 2.0 ML Mn/Co might be explained by unfavorability of large Mn ensembles to be in a HCP configuration. Evidence of this can be seen in Fig. 3, where Mn readily alloys with Co. For both 1.0 ML and 2.0 ML Mn/Co, the binding of $C_{(ad)}$ + $O_{(ad)}$

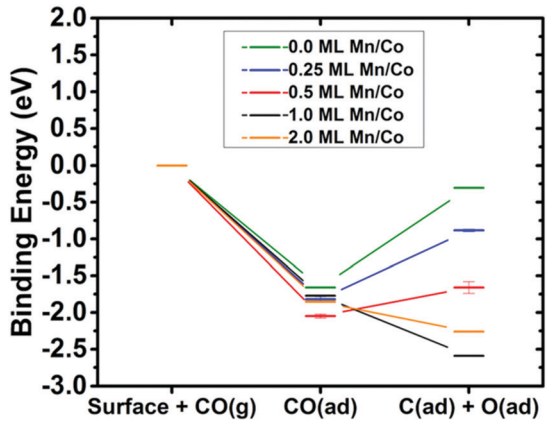

Fig. 4 Schematic energy diagram of molecular CO adsorption and dissociated CO adsorption on Mn/Co surfaces.

is stronger than the binding of molecular CO. The observed increase of calculated binding energy of $C_{(ad)}$ + $O_{(ad)}$ on Mn promoted surfaces aligns with the higher recombinative desorption temperature seen experimentally (Fig. 1a). Past work by Andreoni and Varma suggests that the boundary between molecular adsorption and dissociative adsorption of CO is mildly dependent on the molecular CO chemisorption energy and mostly dependent on the chemisorption energies of dissociated $C_{(ad)}$ and $O_{(ad)}$.[29] Our findings that $C_{(ad)}$ + $O_{(ad)}$ adsorb more strongly to Mn/Co surfaces align with our measurements showing that increased coverages of Mn on Co have higher fractions of dissociated CO that then recombinatively desorb at higher temperatures. These results also suggest that CO is dissociatively adsorbing on our Mn promoted surfaces, which is in agreement with the RAIRS findings reported here (Fig. 1b).

In summary, Mn annealed and alloyed with Co(poly) was seen to increase the dissociative adsorption of CO. Infrared spectroscopy showed decreased molecular CO vibrations on Mn covered surfaces, which is consistent with TPD findings from CO impingement experiments that showed Mn promoted recombinative desorption of CO. By holding our sample at temperatures above the molecular CO desorption temperature, we were able to show minimal change in recombinative desorption intensity, suggesting that dissociated CO states become populated at low temperature. Lastly, DFT calculations show that Mn covered Co(0001) models have increased molecular CO binding energy and increased $C_{(ad)}$ + $O_{(ad)}$ binding energy, which correlates with the presence of dissociated CO on our samples. These findings show that metallic Mn exhibits promoter effects in model Fischer–Tropsch catalysts.

We are thankful for the generous support of the Department of Energy Basic Energy Sciences, Catalysis Science Program (Grant DE-SC0018116 (C. B. M.) and Grant DE-SC0010576 (G. H.)) and the Welch Foundation (Grant F-1436 (C. B. M.) and Grant F-1841 (G. H.)). S. H. was partially supported by the Dorothy Banks Fellowship. Computational resources were provided by the Texas Advanced Computing Center and the National Energy Research Scientific Computing Center.

Conflicts of interest

There are no conflicts to declare.

Notes and references

1 H. Mahmoudi, M. Mahmoudi, O. Doustdar, H. Jahangiri, A. Tsolakis, S. Gu and M. LechWyszynski, *Biofuels Eng.*, 2017, **2**, 11–31.
2 H. Jahangiri, J. Bennett, P. Mahjoubi, K. Wilson and S. Gu, *Catal. Sci. Technol.*, 2014, **4**, 2210–2229.
3 J. Yang, W. Ma, D. Chen, A. Holmen and B. H. Davis, *Appl. Catal., A*, 2014, **470**, 250–260.
4 Shell Investors' Handbook - Financial and Operational Information 2011–2015, 2015.
5 H. M. Torres Galvis and K. P. De Jong, *ACS Catal.*, 2013, **3**, 2130–2149.
6 J. Su, H. Zhou, S. Liu, C. Wang, W. Jiao, Y. Wang, C. Liu, Y. Ye, L. Zhang, Y. Zhao, H. Liu, D. Wang, W. Yang, Z. Xie and M. He, *Nat. Commun.*, 2019, **10**, 1297.
7 E. Ø. Pedersen, I. H. Svenum and E. A. Blekkan, *J. Catal.*, 2018, **361**, 23–32.
8 Y. Yang, T. Lin, X. Qi, F. Yu, Y. An, Z. Li, Y. Dai, L. Zhong, H. Wang and Y. Sun, *Appl. Catal., A*, 2018, **549**, 179–187.
9 T. E. Feltes, L. Espinosa-Alonso, E. de Smit, L. D'Souza, R. J. Meyer, B. M. Weckhuysen and J. R. Regalbuto, *J. Catal.*, 2010, **270**, 95–102.
10 G. R. Johnson, S. Werner and A. T. Bell, *ACS Catal.*, 2015, **5**, 5888–5903.
11 F. Morales and B. M. Weckhuysen, *Catalysis*, 2006, **19**, 1–40.
12 L. Zhong, F. Yu, Y. An, Y. Zhao, Y. Sun, Z. Li, T. Lin, Y. Lin, X. Qi, Y. Dai, L. Gu, J. Hu, S. Jin, Q. Shen and H. Wang, *Nature*, 2016, **538**, 84–87.
13 F. Morales, D. Grandjean, F. M. F. de Groot, O. Stephan and B. M. Weckhuysen, *Phys. Chem. Chem. Phys.*, 2005, **7**, 568–572.
14 F. Morales, D. Grandjean, A. Mens, F. M. F. De Groot and B. M. Weckhuysen, *J. Phys. Chem. B*, 2006, **110**, 8626–8639.
15 F. Morales, F. M. F. De Groot, P. Glatzel, E. Kleimenov, H. Bluhm, M. Hävecker, A. Knop-Gericke and B. M. Weckhuysen, *J. Phys. Chem. B*, 2004, **108**, 16201–16207.
16 D. W. Flaherty, N. T. Hahn, D. Ferrer, T. R. Engstrom, P. L. Tanaka and C. B. Mullins, *J. Phys. Chem. C*, 2009, **113**, 12742–12752.
17 G. Bardi, U. Tiscione and P. Rovina, *Appl. Surf. Sci.*, 1986, **27**, 299–317.
18 P. Vaari, J. Vaara, T. Lahtinen and J. Hautojarvi, *Appl. Surf. Sci.*, 1994, **81**, 289–297.
19 F. Morales, E. de Smit, F. M. F. de Groot, T. Visser and B. M. Weckhuysen, *J. Catal.*, 2007, **246**, 91–99.
20 G. A. Beitel, A. Laskov, H. Oosterbeek and E. W. Kuipers, *J. Phys. Chem.*, 1996, **100**, 12494–12502.
21 L. E. S. Rygh, O. H. Ellestad, P. Klaeboe and C. J. Nielson, *Phys. Chem. Chem. Phys.*, 2000, **2**, 1835–1846.
22 S. A. Stevenson, A. Lisitsyn and H. Knözinger, *J. Phys. Chem.*, 1990, **94**, 1576–1581.
23 Y. Iijima, K. I. Hirano and O. Tagijchi, *Philos. Mag.*, 1977, **35**, 229–244.
24 G. Attard and C. Barnes, *Surfaces*, 1998, pp. 43–47.
25 A. E. Ray, S. R. Smith and J. D. Scofield, *J. Phase Equilib.*, 1991, **12**, 644–647.
26 R. Tran, Z. Xu, B. Radhakrishan, D. Winston, W. Sun, K. A. Persson and S. P. Ong, *Sci. Data*, 2016, **3**, 160080.
27 C. P. Gazzara, R. M. Middleton, R. J. Weiss and E. O. Hall, *Acta Crystallogr.*, 1967, **22**, 859–862.
28 W. Wang, Z. Hou, R. Lizárraga, Y. Tian, R. P. Babu, E. Holmström, H. Mao and H. Larsson, *Acta Mater.*, 2019, **176**, 11–18.
29 W. Andreoni and C. M. Varma, *Phys. Rev. B: Condens. Matter Mater. Phys.*, 1981, **23**, 437–444.

